Water resources remain sustainable in global revegetated regions

Authors: Yuanfang Chai [a,b,c], Yao Yue [d*], Alistair GL Borthwick [e,f], Yichu Wang [g], Louise Slater [h], Dunxian She [d], Dongpu Feng [i], Chiyuan Miao [a*]

Affiliations:

[a] State Key Laboratory of Earth Surface Processes and Disaster Risk Reduction, Faculty of Geographical Science, Beijing Normal University, Beijing 100875, China

[b] College of Geography and Environmental Sciences, Zhejiang Normal University, Jinhua, 321004, China

[c] China-Mozambique Belt and Road Joint Laboratory on Smart Agriculture, Zhejiang Normal University, Jinhua 321004, China

[d] State Key Laboratory of Water Resources and Hydropower Engineering Science, School of Water Resources and Hydropower Engineering, Wuhan University, Wuhan, 430072, China

[e] School of Engineering, The University of Edinburgh, The King's Buildings, Edinburgh EH9 3JL, UK

[f] School of Engineering, Mathematics and Computing, University of Plymouth, Drake Circus, Plymouth PL4 8AA, UK

[g] College of Water Science, Beijing Normal University, Beijing, 100875, China

[h] School of Geography and the Environment, University of Oxford, South Parks Rd, Oxford, OX1 3QY, UK

[i] School of Civil and Hydraulic Engineering, Ningxia University, Yinchuan, 750021, China

***Corresponding authors**: Yao Yue (+86-15927346027, yueyao@whu.edu.cn) and Chiyuan Miao (+86-10-58804191, miaocy@bnu.edu.cn)

Abstract

Intense debate surrounds the question of whether transpiration from revegetated regions may exacerbate water shortages globally. Using outputs from 20 CMIP6 models for 1982–2016 and 2030–2100 alongside observations, we find that the water resources remaining after subtracting increased evapotranspiration from rainfall and meltwater from snow and glaciers exceeded human usage during 1982–2016 across almost three quarters (72.2%) of global revegetated regions. CMIP6 projections for 2030–2100 indicate that human water demand is likely to be met in 79.4% of revegetated regions, but India and Oceania warrant attention because of possible precipitation decline and/or population growth. Approximately 1.6% of currently bare regions (40.6×10^4 km^2) in Canada, Central Asia, and the fringes of deserts have adequate water for revegetation over 2030–2100. These findings underscore the necessity of strategic water management and monitoring in revegetated areas to balance ecological benefits with human water needs.

Keywords: global revegetation; water supply; water consumption; water resources sustainability; CMIP6.

1 Introduction

Revegetation, undertaken worldwide as a carbon sequestration strategy for mitigating climate change [1], has vast consequences for water and carbon cycles from local to global scales [2]. Revegetation plays an important role in enhancing soil stability, preventing soil erosion, reducing desertification, attenuating flood flow, and increasing agricultural outputs [3–4]. During 1982–2016, global vegetation cover increased by 7.1%, i.e. 2.24 million km^2 [5], and a further 9 million km^2 of revegetation is planned ([6], Fig.1a). Such widespread, intensive ecological restoration is an indispensable pathway for limiting global warming [7]. However, new vegetation cover also increases water consumption through transpiration and interception processes ([8–9], Fig. 1b, c and d), thus creating potential competition between vegetation and humans for water resources, especially in arid areas [10].

The potential impact of revegetation on the water cycle has sparked debate over whether humans should continue greening the land surface of the Earth. Many scientists argue that increased evapotranspiration from revegetation reduces surface runoff and soil moisture [11–13], challenging the sustainability of water resources [10, 14]. Some experts have even suggested that the world's largest-scale afforestation activities in semi-arid or arid areas of China may have unsustainable effects on water resources in the long run [15]. By contrast, others argue that increased evapotranspiration due to land greening raises air humidity and local rainfall ([16–17], Fig. 1c), thereby compensating for enhanced water loss by evapotranspiration [18]. Furthermore, they find that increased vegetation coverage can improve the stability and water-holding capacity of soils [19]. It is not straightforward to resolve the debate, given that the processes of runoff generation and concentration are radically changed by transitions

in land cover [20]. Moreover, the long-term effects of climatic changes in precipitation and temperature generate additional uncertainty when projecting the influence of revegetation on the water cycle [21].

One possible approach to resolve the controversy is to estimate the regional water balance between water consumption and water supply from different pathways before and after revegetation [22]. If water supply is sufficiently abundant to support both vegetation growth and human society over a relatively long period following revegetation, then water resources are unlikely to be strained by local revegetation. In this study, we assemble outputs from 20 bias-corrected CMIP6 models and other observational datasets for rainfall, meltwater from snow and glaciers, evapotranspiration, transpiration, Leaf Area Index (LAI), and water consumption for human use during 1982–2016 and 2030–2100 (Materials and Methods and Table S1 online) to determine whether global greening is likely to be sustainable in the context of water resources management (Fig. 1c-d). By incorporating soil constraints (including soil organic carbon, pH, nitrogen, and cation exchange capacity) and climatic treeline thresholds, we further assess the potential for future afforestation on existing bare lands. Our study provides critical insights into the sustainability of global revegetation efforts by evaluating the balance between water supply and demand under future climate scenarios, thereby informing policy decisions on ecological restoration and water resource management.

2 Materials and Methods

2.1 Classification of global land cover change

Based on the annual average vegetation cover fraction (CF) (Eq. (1)) and the

classification criteria of the International Geosphere-Biosphere Programme (IGBP), the Earth's land surface was divided into five categories. Areas with less than 10% vegetation cover during the whole period (1982–2016) were labelled as 'continuously bare regions'. Areas with more than 10% vegetation cover during the whole period were labelled as 'continuously vegetated regions'. Land changing from bare to vegetated status once during the whole period (or with multiple shifts between bare and vegetated regions before becoming vegetated during the final five years) was labelled 'revegetated regions'. Land changing from vegetated regions into bare regions only once (or with multiple shifts but which became bare in the final five years) was labelled 'devegetated regions'. The remaining land which underwent multiple mutual transformations and remained unstable during the final 5 years was labelled 'frequently changing regions'. The annual average vegetation cover fraction of a given grid cell was calculated using the Beer's Law approximation [23]:

$$CF = 1 - e^{-LAI/2} \quad (1)$$

where *LAI* is the Leaf Area Index which was obtained from NOAA Climate Data Record of AVHRR Leaf Area Index from 1982 to 2016 at a spatial resolution of 0.05°×0.05°.

2.2 Estimate of water consumption driven by vegetation growth and atmospheric evaporative demand during 1982–2016 and 2030–2100

Water consumption related to vegetation growth and evaporation comprises observed evapotranspiration, which can be separated into transpiration, interception loss, bare soil evaporation, snow sublimation, and open water evaporation [24] (Eq. (2)). Among these, transpiration (E_t) gives an estimate of water consumption for vegetation growth, while the combined total of interception loss, bare soil evaporation, snow sublimation,

and open water evaporation represents evaporation of water converted from liquid to vapor, lost to the atmosphere from various surfaces (E_c, Eq. (3)). Compared with the period before re-vegetation activities, changes in E_t during the period after re-vegetation activities (ΔE_t, Eq. (4)) are caused by increased water demand by newly planted trees, while differences in E_c (ΔE_c, Eq. (5)) are primarily driven by climate change, especially rising temperature [25].

$$ET = E_t + E_i + E_b + E_s + E_w \quad (2)$$

$$E_c = E_i + E_b + E_s + E_w \quad (3)$$

$$\Delta E_t = E_{t\_post} - E_{t\_pre} \quad (4)$$

$$\Delta E_c = E_{c\_post} - E_{c\_pre} \quad (5)$$

where ET is evapotranspiration (mm); E_t is transpiration (mm); E_i is interception loss (mm); E_b is bare soil evaporation (mm); E_s is snow sublimation (mm); E_w is open water evaporation (mm); E_c is water consumption for atmospheric evaporative demand (mm); ΔE_t is increased water consumption for new vegetation cover (mm); and ΔE_c is increased water consumption for increased atmospheric evaporative demand (mm).

Monthly data on transpiration and interception losses, bare soil evaporation, snow sublimation, and open water evaporation during 1982–2016 were obtained from the Global Land Evaporation Amsterdam Model datasets (GLEAM) at a spatial resolution of 0.25°× 0.25°. Monthly data during 2030–2100 on total evapotranspiration and transpiration were obtained from 20 CMIP6 models under SSP245 (see specific model names in Table S1 online). The choice of SSP245 is based on its alignment with realistic emission trajectories, representing a moderate level of greenhouse gas emissions and socio-economic development expected in the coming decades. This scenario provides

a solid framework for assessing potential climate impacts and developing effective adaptation strategies.

2.3 Revegetation sustainability in terms of water supply and water consumption

Whether revegetated regions are sustainable can be determined by analyzing the balance between water supply and water consumption in both the current and future periods. The water balance equation is given by

$$\Delta W = R + MW - ET - H \quad (6)$$

where R is rainfall (mm); MW is surface meltwater from snow and glaciers (mm); ET is evapotranspiration (mm); and H is human water consumption (mm). Following Khan et al., [1], human water consumption encompasses domestic water use (D_{we}: water used for household activities, including drinking, sanitation, and other residential needs), irrigation (I_{we}: water used for agricultural irrigation across 13 crop types), water for electricity generation (E_{we}: water used for cooling in thermal and nuclear power plants, allocated monthly based on electricity demand and cooling/heating degree days), livestock needs (L_{we}: water used for drinking and management of cattle, buffalo, sheep, goats, pigs, and poultry), industrial and manufacturing purposes (LM_{we}: water used for manufacturing and production processes), and mining (M_{we}: water used for mineral extraction) (Eq. (7)).

$$H = D_{we} + I_{we} + E_{we} + L_{we} + IM_{we} + M_{we} \quad (7)$$

In addition to the evapotranspiration data source described in the previous section, data on water supply from rainfall and meltwater, and human water consumption during 1982–2016 and 2030–2100 were also collected. Observation-based monthly precipitation data during 1982–2016 were obtained from the Global Precipitation Climatology Centre (GPCC) at a spatial resolution of 0.25°× 0.25°. By excluding

169 precipitation at temperatures below freezing, rainfall data during 1982–2016 essential
170 to this analysis were isolated. Observation-based monthly meltwater data were
171 collected from ERA5-land. For the period of 2030–2100, monthly precipitation and
172 meltwater data were obtained from 20 CMIP6 models (see specific model names in
173 Table S1 online) under SSP245. Similarly, by excluding snowfall, rainfall data for
174 2030–2100 were extracted. Data on the monthly human water consumption were
175 obtained from the Joint Global Change Research Institute (JGCRI).
176
177 The dataset of human water consumption was generated by coupling the Global Change
178 Analysis Model (GCAM), a land allocation downscaling model, and a water demand
179 downscaling model [26]. It provides global sectoral water withdrawals and
180 consumption at a 0.5-degree resolution and monthly timestep for 2010–2100. Its key
181 strengths include: It integrates not only climate variables but also critical
182 socioeconomic drivers. GCAM explicitly simulates future population growth,
183 urbanization and economic development, represented through five Shared
184 Socioeconomic Pathways (SSPs). These integrated socioeconomic considerations are
185 reflected in Fig. S1 (online), which displays the annual water consumption distribution
186 across domestic, electricity, irrigation, livestock, manufacturing, and mining sectors.
187 Most critically, Figs. S2–S3 (online) provide further granularity by disaggregating
188 irrigation water use into 13 major crop categories (including corn, wheat, rice, and oil
189 crops). This enables direct quantification of water demands driven by future food
190 production and analysis of crop mix impacts. The dataset directly provides gridded
191 domestic water use (reflecting urban household demand) and manufacturing water use
192 (reflecting urban industrial activity). Its spatial downscaling uses population and
193 livestock distribution grids, implicitly linking population density (i.e., urbanization) to

spatial water demand patterns. GCAM outputs were calibrated against regional-scale observed data for the base year. A core validation step reaggregated the downscaled gridded monthly results to the original GCAM regions and annual timesteps. Comparisons confirmed the algorithms introduced no numerical errors, preserving the original inputs' totals and spatiotemporal patterns [26]. For 2010, the dataset's outputs were compared against two authoritative historical global water use datasets [27–28]. Despite differences in sources and methodologies (e.g., study periods, sector definitions, hydropower accounting), results showed substantial consistency in spatial distribution and seasonal variation, strongly supporting methodological robustness.

2.4 Maximum coverage fraction for future re-vegetation of currently bare regions

An opportunity exists for re-vegetation of currently bare regions benefiting from extra water resources (i.e. water supply exceeding water consumption) in the future. To evaluate the maximum potential for vegetation restoration in such regions, a regression relationship was developed between the change in vegetation cover fraction (ΔCF in %, all types of vegetation are included) and the change in water consumption for vegetation growth through transpiration and interception processes (ΔE_v) in bare regions during 1982–2016 (Eq. (8)). The regression models (Eqs. (8)–(9)) were trained using grid-level historical time series (1982–2016) of vegetation cover fraction (derived from AVHRR LAI) and water consumption (from GLEAM v3.2 transpiration and interception data) for each 0.5° grid cell.

Based on these regression relationships and an assumption that the newly increased future supply-demand gap (ΔW) can be fully utilized for further revegetation, the maximum potential for revegetation (ΔCF_{max}) was estimated from Eq. (9). The change

in vegetation cover fraction (%) is given by

$$\Delta CF = a \cdot \Delta E_{\mathrm{v}} + b \tag{8}$$

where ΔE_{v} is the change in water consumption for vegetation growth through transpiration and interception processes (mm); and a and b are the slope and intercept values of the linear regression equation. The maximum potential increased vegetation cover fraction in currently bare regions (%) is similarly expressed:

$$\Delta CF_{\max} = a \cdot \Delta W + b \tag{9}$$

where ΔW is the water supply-demand gap (mm).

Uncertainty in the regression coefficient (slope value a in Eq. (9)) can lead to uncertainty in the predicted potential for revegetation. Here we use Eq. (10) to estimate the standard error of a, which is used in analyzing uncertainty for the predicted cover fraction in the future.

$$\sigma_a^2 = \frac{\frac{1}{N-2}\sum_{n=1}^{n=N}(y_n - f_n)^2}{\sqrt{N}\sum_{n=1}^{n=N}(x_n - \bar{x})^2} \tag{10}$$

where N is the number of data points; f_n is calculated using Eq. (9) for a given time series of x_n; y_n is the observed time series of ΔCF; and $\bar{x}$ is the mean value of the time series of x_n.

Soil constraints, such as low organic carbon, extreme pH levels, insufficient nitrogen, or poor cation exchange capacity, can severely limit plant growth and survival, even if water supply is adequate. Similarly, climatic treeline constraints, determined by

243 growing season temperature, define the thermal limits for vegetation establishment.
244 Regions beyond these thresholds are unsuitable for afforestation due to physiological
245 stress on plants, regardless of water availability. Therefore, we further integrate high-
246 resolution (250-meter) soil parameters from the SoilGrids dataset [including soil
247 organic carbon (Fig. S4a online), pH values (Fig. S4b online), nitrogen content (Fig.
248 S4c online), and cation exchange capacity (Fig. S4d online)] with climatic treeline
249 constraints derived from ERA5-Land temperature data (Fig. S5 online; defined by
250 growing season temperature in revegetated regions, as these areas reflect suitable
251 climatic conditions for afforestation) to evaluate the future afforestation potential of
252 bare lands under projected water availability. By combining these factors with water
253 resource projections, we provide a more realistic assessment of revegetation potential
254 in currently bare regions. This multi-criteria approach ensures that afforestation
255 strategies account not only for hydrological feasibility but also for long-term ecological
256 sustainability under changing environmental conditions.
257
258 **2.5 CDF-t bias correction method**
259 The future climate projections from CMIP6 models have considerable uncertainty [29],
260 highlighting the need for bias correction methods to better capture changes in water
261 supply and consumption within revegetation areas. In our analysis, we apply bias
262 correction to future monthly evapotranspiration, rainfall, meltwater from snow and
263 glaciers, and transpiration projected by the 20 CMIP6 models for the period 2030–2100.
264 The observed data used for this process is sourced from GLEAM (for
265 evapotranspiration and transpiration), GPCC (for rainfall), and ERA5-land (for
266 meltwater).
267

The CDF-t statistical bias correction method used in this study employs a transfer function that connects the cumulative distribution function (CDF) of large-scale variables with the CDF of observed data. We denote F_{SH} as the CDF of monthly average observations at a specific site during the modeling phase, while F_{GH} refers to the CDF of the output from the large-scale atmospheric circulation model, interpolated to that location over the same timeframe [30]. F_{SF} and F_{GF} represent the CDFs of observed and simulated monthly average climate variables during the validation phase, respectively. We postulate that a transfer function T can be defined during the validation phase, allowing the CDF of model-simulated climate variables to align closely with the observed climate variables, thus enabling effective bias correction [30].

$$T\left(F_{GH}(X)\right) = F_{SH}(u) \tag{11}$$

Next, we define $u = F_{GH}(X)$. As a result, we can express $X = F_{GH}^{-1}(u)$. The variable u is constrained within the range [0, 1]. Substituting X into Eq. (11) provides us a simplified form for the transfer function.

$$T(u) = F_{SH}\left(F_{GH}^{-1}(u)\right) \tag{12}$$

The transfer function T represents the relationship between the CDF of historical observations during the modeling phase and that of the atmospheric circulation model. If we assume that this transfer function remains valid during the validation period, we can apply it to the large-scale variables produced by the climate model to achieve regional bias-corrected results [30], represented as follows:

$$T\left(F_{GF}(X)\right) = F_{SF}(X) \tag{13}$$

$$F_{SF}(X) = F_{SH}\left(F_{GH}^{-1}\left(F_{GF}(X)\right)\right) \tag{14}$$

The transfer function plays a crucial role in establishing the functional relationship between the CDF of historical observations and the CDF of the model for a particular value of X. This relationship is anticipated to persist into the future, facilitating the derivation of the bias-corrected CDF.

In this study, the historical timeframe spanning 1982 to 2014 (the CMIP6 historical data extends only until 2014), totaling 33 years, is divided into two distinct segments. The initial 16 years (1982 to 1997) are designated as the modeling phase, where the statistical bias-corrected relationship is developed using both observational and model data. The following 17 years (1998 to 2014) serve as the validation phase, evaluating the accuracy of the statistical bias-corrected results. It is crucial to note that a longer modeling phase contributes to a more reliable functional relationship between observational and model data. Consequently, for future projections covering the period from 2030 to 2100, the modeling phase is extended to include the full range from 1982 to 2014. This extension facilitates a thorough analysis of the bias-corrected results under the SSP245 scenario.

Fig. S6 (online) presents the observed and simulated (before and after bias correction) global annual mean evapotranspiration, rainfall, meltwater and transpiration during the validation period from 1998 to 2014. Prior to bias correction, the original CMIP6 models significantly overestimated the global annual mean values of evapotranspiration (Fig. S6a online), meltwater (Fig. S6b online), and rainfall (Fig. S6c online), while underestimating transpiration (Fig. S6d online). After bias correction, the discrepancies between the simulated climate data and observations were substantially reduced,

achieving a decrease of 87%–97% compared to pre-correction values (Fig. S6 online and Fig. S7 online). Following bias correction, the spatial distributions of these climate variables closely align with observations (Fig. S8 online), indicating the effectiveness of the correction process. This improved alignment enhances our confidence in the bias-corrected results for the future period of 2030–2100.

3 Results and Discussion

3.1 Global distribution of revegetated regions

Fig. 1a classifies the Earth's land surface into five categories of land cover change during 1982–2016, i.e. Continuously vegetated regions, Continuously bare regions, Revegetated regions derived from originally bare regions, Devegetated regions reflecting changes to originally vegetated regions, and Frequently changing regions which alternate between vegetated and bare regions during the time period of interest. The revegetated region pattern is widespread globally, covering 18.9% of the world's land surface (2558.8×10^4 km^2, Table S2 online). Revegetated regions are partly distributed in regions where large-scale revegetation activities by humans have occurred, such as the Great Green Wall at the southern border of the Sahara Desert, North Africa [31], the Grain to Green Program in the Loess Plateau of China [10], the government promoted tree-planting programs in the Great Indian Desert and the Deccan Plateau of India [32], and the cropland reclamation project in Australia [33]. Natural factors also lead to revegetation of land, as in the cases of North Asia and the northern part of North America where permafrost has retreated rapidly due to global warming [34–35]. At the global scale, revegetated regions are mainly located in the northern hemisphere (70% of the total revegetated region), especially in Asia (50%) and North America (15%), and are relatively sparse in Africa (11%), Oceania (10%), and South

America (9%).

3.2 Changes in water consumption of revegetated regions

Over the period 1982–2016, 75.2% (1915.0×10^4 km^2) of revegetated regions presented an increase in annual evapotranspiration after revegetation, with a mean change of 26.4 mm (Fig. 2a). Of the increased annual water consumption, 72.3% (19.1 mm, Fig. S9a online) was taken up by transpiration by new vegetation cover [36] (E_V), and 27.7% (7.3 mm) by water evaporation (E_C). Observations indicate that the mean land surface temperature of revegetated regions increased by 1.5 ℃ during 1982–2016. Despite this warming trend [37–38], water evaporation only increased across 61% of the total revegetated regions. The remaining 39% of the revegetated regions experienced decreasing water evaporation, largely owing to soil-moisture limitations on evaporative capacity [39]. In permafrost regions, rising water evaporation was more common (78% of all permafrost areas), primarily because wetland water tables became elevated close to the ground surface due to rapid thawing [40–42]. Seasonally, during the peak growing periods of revegetated vegetation—specifically, from May to October in the Northern Hemisphere and from November to April in the Southern Hemisphere—water consumption for evapotranspiration reaches its highest levels, accounting for 59.2%–68.1% of the total annual consumption (Fig. S10 online). During these months, enhanced photosynthetic activity and vegetation growth significantly increase water uptake, creating a pronounced demand for water resources.

The remaining 24.8% of revegetated regions with decreased evapotranspiration are predominantly located in South Central Australia (Fig. 2a). In these regions, a downward trend in soil moisture has contributed to the suppression of

evapotranspiration [39]. Here, the average reduction in annual evapotranspiration was 7.2 mm. In Fig.2a, the areas covered by large-scale tree-planting programs in the Loess Plateau of China, the Great Indian Desert, the Deccan Plateau of India and the Great Green Wall of North Africa have experienced increasing trends in evapotranspiration over the past 40 years mainly due to afforestation (contributing over 89%), with increases in evapotranspiration by 15%–19%, far above the average increases of all the revegetated regions (4.0%).

During 2030–2100, annual average evapotranspiration is projected to further increase to 543.9 ± 18.5 mm (Fig. 2b) in the world's revegetated regions. In 71.8% ± 9.4% of the revegetated regions, evapotranspiration may rise considerably, with a mean annual increment of 25.2 ± 8.2 mm (Fig. 2b). Increased vegetation-related transpiration processes, as indicated by the growing LAI in the revegetated regions from 1.33 ± 0.29 in 2030 to 1.54 ± 0.44 in 2100 (mean values of the outputs from 20 CMIP6 models under SSP245), are expected to drive 78.5% ± 14.3% of the increase in evapotranspiration in revegetated regions (Fig. S9b online). The remaining increment of 5.4 mm in annual evapotranspiration is primarily attributed to increased water evaporation. Similarly, regions such as the Loess Plateau of China (38.9 ± 11.7 mm) and the Great Green Wall of North Africa (28.6 ± 6.0 mm) are projected to experience the largest annual increases in evapotranspiration. Conversely, in 28.2% of the revegetated regions (including Australia and southern Africa), annual evapotranspiration is estimated to decrease by an average of 7.8 ± 3.5 mm, partly due to limited water supply for evapotranspiration from the soil.

3.3 Changes in water supply of the revegetated regions

392 Annual rainfall is the most important pathway of water supply for most of the world's
393 revegetated regions. During 1982–2016, about 67.6% of the revegetated regions
394 (1722×10^4 km^2) experienced a mean increase of 57.1 mm in yearly rainfall after
395 revegetation (Fig. 2c). This increase was primarily concentrated in the mid-latitude
396 regions of Asia, including the coastal areas of India and China, as well as in parts of
397 South America, Africa, and central Australia. Areas with the highest rainfall increases
398 would have witnessed groundwater recharge, driving an upward trend in vegetation
399 greenness [43–44], especially in arid and semiarid areas. In the remaining 32.4% of
400 revegetated regions, mean annual water rainfall decreased by 18.1 mm on average, with
401 the largest extent of reduction occurring in Australia, particularly in newly reclaimed
402 cropland areas (Fig. 2c). Annual meltwater from snow and glaciers also provides an
403 important pathway for water supply, especially in the Arctic Circle and areas with high
404 snow-capped mountains (Fig. 2e). In Fig. 2e, our analysis indicates that the mean annual
405 meltwater from snow and glaciers decreased by 6.9 mm in 88.1% of the revegetated
406 regions, most notably in the Middle and high latitudes of the Northern Hemisphere,
407 Andes Mountains and Tibetan Plateau, and increased by 1.0 mm on average in the
408 remaining 11.9% of the revegetated regions. Changes in meltwater exert persistent
409 effects on soil moisture, especially in grasslands, regulating the local vegetation growth
410 rate [45]. By considering both rainfall and meltwater, we estimate that the total water
411 supply increased after revegetation in 55.8% of the revegetated regions (Fig. S11a
412 online). Notably, this increase was observed in the Great Green Wall in North Africa,
413 reclaimed land in Australia, the tree-planting initiative in the Great Indian Desert-
414 Deccan Plateau, and various revegetated regions in South America.
415
416 Global rainfall is projected to change radically in the future period of 2030–2100. Mean

annual rainfall is projected to rise from 822.8 mm during 1982–2016 to 840.1 ± 8.4 mm in the revegetated regions (Fig. 2d), 66.1% ± 11.7% of which is predicted to experience an even sharper increase of 45.4 ± 5.1 mm, including the Great Green Wall in North Africa, the tree-planting program in the Great Indian Desert-Deccan Plateau, the Grain to Green Program area of the Loess Plateau, China and the tree-planting initiative in the Great Indian Desert-Deccan Plateau (Fig. 2d). This significant increase would primarily arise from maintaining the energy balance under increased temperature in the future period. In a warming climate, radiative energy in the atmosphere is likely to decrease with increasing longwave emission [46]. The energy balance can thus only be maintained if rainfall intensifies and atmospheric latent heat increases [47]. This process of re-establishing the energy balance is supported by the land-surface energy conservation equation [46]. However, in the Northern Hemisphere, the increase in rainfall is predominantly observed during the non-growing season (November to April), while a decline is evident during the growing season. This pattern may be associated with the phenomenon where wet areas become wetter and dry areas become drier, particularly in arid and semi-arid regions. Such shifts could worsen water scarcity in these areas, leading to increased stress on ecosystems and agricultural practices that depend on consistent water supply. The decline in rainfall during the growing season raises significant concerns about whether available moisture will be sufficient to meet the heightened water demand during critical periods of plant growth. Throughout the remaining area of the revegetated regions, a significant drop of 24.4 ± 6.3 mm in yearly rainfall is projected to occur in areas including the reclaimed land in Australia. Changes in meltwater from snow and glaciers are expected to affect almost all the revegetated regions within the latitudes of 24°–90°N in the North Hemisphere (Fig. 2f). Tibetan Plateau, Sweden, Finland, and Canada are projected to experience a sharp decrease in

meltwater of 19.3 ± 5.7 mm (60°–90°N), whereas an increase of 23.1 ± 12.4 mm is predicted to occur in Siberia, on average. The increased meltwater in Siberia mainly attributes to atmospheric dynamic-induced moisture convergence, involving the effects of vertical motion and horizontal convection of moisture [48]. Overall, future changes in rainfall are the primary driver of projected variations in total annual water supply across revegetated regions, resulting in an increase in total water supply for most areas. However, decreases in total water supply were also noted in Australia and southern Africa (Fig. S11b online), which could have profound implications for agricultural productivity and ecosystem health, particularly in regions where water availability is already limited. Other regions, such as the Mediterranean and southern South America, have also experienced reductions. However, these areas have limited vegetation.

3.4 Water resource sustainability in revegetated region

To evaluate the sustainability of water resources in revegetated regions, we analyze whether the difference between regional water supply and natural water consumption by vegetation can adequately support human needs in agriculture, industry, and daily life. By examining historical data on evapotranspiration, rainfall, and meltwater from snow and glaciers, we found that the difference between water supply and natural water consumption—termed the natural water resource surplus—remained relatively stable over the past 40 years post-land cover transition, with the annual mean surplus increasing slightly from 300.6 mm to 311.3 mm (Fig. 3a). Notably, an increase of more than 39.5 mm in natural water resource surplus occurred in 44.5% of the revegetated regions, primarily in South America, the Great Green Wall of North Africa, Kalimantan Island, and Southwest China. Conversely, a decrease of over 28.9 mm was observed in Siberia and South China, where reductions in meltwater coincided with a significant

rise in evapotranspiration. With more pronounced climate variations expected between 2030 and 2100, the natural water resource surplus is likely to experience significant changes (Fig. 3b). On average, this surplus is projected to increase by 28.6 ± 7.4 mm annually in 53.5% ± 8.6% of the revegetated regions, particularly in East and Southeast Asia, India, the Great Green Wall of North Africa, and Siberia (Fig. 3b). This increase could enhance water availability for agriculture and other human uses in these regions. In contrast, the remaining revegetated regions are anticipated to see a decline in the natural water resource surplus by as much as 26.2 ± 11.2 mm, predominantly affecting Australia, where reduced water availability may pose challenges for both ecosystems and human activities.

The sustainability of water resources is increasingly threatened by rising human water consumption. Based on global gridded monthly water withdrawal and consumption [49] (Fig. 4; note that this dataset lacks human water use prior to 2010), we estimated a significant upward trend in total human water consumption in the 83.7% of the revegetated regions ($P < 0.01$) from 2010 to 2016, with an annual increase of 365.2 ± 6.6 × 10^3 m^3 a^{-1} (Fig. 4a and b, and Table S3 online). The most pronounced increase was observed in irrigation water use for revegetation and agricultural crops, which rose by 244.3 ± 6.4 × 10^3 m^3 a^{-1} (Fig. 4e). This was followed by livestock water use (54.5 ± 0.7 × 10^3 m^3 a^{-1}, Fig. 4g), industrial and manufacturing water use (26.7 ± 0.5 × 10^3 m^3 a^{-1}, Fig. 4h), domestic water use (19.8 ± 0.3 × 10^3 m^3 a^{-1}, Fig. 4d), electricity generation water use (16.2 ± 0.1 × 10^3 m^3 a^{-1}, Fig. 4f), and mining water use (3.7 ± 0.1 × 10^3 m^3 a^{-1}, Fig. 4i). The largest increments in water use were observed in India, East China, North and Central Africa, and coastal regions of South America (Fig. 4b).

During 2030–2100, total human water use is projected to continue increasing at a rate of $136.0 \pm 1.7 \times 10^3$ m^3 a^{-1} (Fig. 4c). The largest increases are irrigation water use for revegetation and agricultural crops ($72.8 \pm 2.1 \times 10^3$ m^3 a^{-1}) and livestock water use ($41.0 \pm 0.3 \times 10^3$ m^3 a^{-1}). Conversely, domestic water use ($-7.1 \pm 0.4 \times 10^3$ m^3 a^{-1}) and mining water use ($-2.7 \pm 0.2 \times 10^3$ m^3 a^{-1}) are expected to decline, potentially due to projected decreases in population and mineral resource extraction. The most significant reductions in these two categories are expected in southeastern China due to population decline. Seasonally, the highest demand for electricity generation water use occurs in the months of June, July, and August, coinciding with peak electricity consumption (Fig. S12 online). Irrigation water use for revegetation and agricultural crops peaks from May to August, aligning with the critical growth season for vegetation, which necessitates substantial water resources.

To evaluate the sustainability of water resources in the revegetated regions, we assess the balance between natural water resource surplus (Fig. 3) and human water consumption (Fig. 4). A positive balance indicates that the natural surplus can adequately support human needs, suggesting sustainable management of water resources. Conversely, a negative balance raises concerns about potential overexploitation and unsustainability. After revegetation activities (Fig. 5a, 2010–2016), we find that the historical annual mean human water use can be satisfied in nearly all the revegetated regions (72.2%). This indicates a positive effective water resource surplus, particularly in South China (695.6 mm), the Tibetan Plateau (334.9 mm), South America (382.0 mm), and high-latitude regions of Asia (169.3 mm). Conversely, in the remaining 17.8% of the revegetated regions, the natural water resource surplus fails to meet human consumption, resulting in a negative effective water resource surplus. This

issue is especially prominent in revegetation regions of India, Australia, and southern Africa. In India, the rapid increase in domestic water use, industrial and manufacturing water use, livestock water use, irrigation water use, and electricity generation water use—driven by population growth—contributes to this demand (Fig. S13 online).

To further strengthen the robustness of our conclusions, we conducted additional validation using high-resolution ERA5-Land climate data (spatially downscaled to 250 m). ERA5-Land, which includes precipitation, temperature, and evapotranspiration variables, has been extensively validated at the site level and is widely recognized in climate, hydrological, and ecological research. As shown in Fig. S14 (online), our ERA5-Land validation results show that the historical annual mean human water use can be satisfied in nearly all the revegetated regions (73.0%). This consistent finding further confirms the validity of our results.

To examine the sustainability of revegetation, we estimate future projections during 2030–2100. After subtracting total human water use from annual natural water surplus, the remaining water resources appear abundant in 79.4% of the revegetated regions, which implies scope for further revegetation activities over the next 80 years (Fig. 5b). However, human water use may not be guaranteed in Northwest India and Southeast Pakistan, most probably due to rapid population growth that is forecast in the next 80 years.

Although water resources are considered sustainable on an annual scale in most revegetated regions (Fig. 5), such that human water use can generally be supported in

both historical and projected future periods, the situation is more complex on a monthly scale. This complexity arises because the peak periods of water usage for vegetation frequently overlap with high human water consumption, particularly in irrigation and hydropower sectors. Consequently, we conducted a detailed analysis of the monthly effective water resource surplus. Our findings reveal that after revegetation (Fig. S15 online, 2010–2016), an average of 44% ± 7.3% of revegetated regions experience a monthly natural water resource surplus insufficient to meet human water demands. This shortfall necessitates the extraction of additional local water resources, such as rivers, lakes, and groundwater, resulting in unsustainable water resource conditions. The regions most severely impacted by this issue include tree-planting initiatives in the Great Indian Desert and the Deccan Plateau in India, as well as the Great Green Wall at the southern border of the Sahara Desert (Fig. S16 online). In these areas, critical shortages are felt in approximately eight months of the year (from January to May and October to December) where the natural water resource surplus is inadequate to support human consumption. This produces significant stress on local water systems during these critical months. Moreover, high-latitude regions in the Northern Hemisphere and revegetated areas in Australia also experience about five months of unsustainable water resources annually. In these regions, the impact of revegetation activities on human water demand remains substantial. In contrast, China, including the Tibetan Plateau, generally maintains sustainable water resources throughout most months of the year, avoiding excessive extraction from local water sources. Looking ahead to the period from 2030 to 2100 (Fig. S17 online), water resources in high-latitude regions of the Northern Hemisphere are expected to improve due to increased rainfall, leading to a reduction in the number of months with unsustainable water resources. Although conditions in the tree-planting programs in the Great Indian Desert and the Deccan

Plateau, as well as the Great Green Wall, show some improvement, seven months of the year (from January to April and October to December) are still likely to experience critical shortages where the natural water resource surplus cannot adequately support human water use. Conversely, revegetated regions in China are projected to continue supporting sustainable water resources throughout most months of the year.

The significant and prolonged period of unsustainability during certain months of the year, despite an annual average that appears sustainable, raises important questions about water resource management. This discrepancy arises because many months experience a natural water resource surplus that is insufficient to meet human water use, resulting in unsustainable conditions. However, during other months, effective water resource surpluses may compensate for these deficits. This balance allows the annual average to remain sustainable. This finding highlights the necessity of evaluating water resource sustainability beyond just annual averages. To accurately assess potential risks of unsustainability, it is crucial to consider higher temporal resolutions such as monthly averages.

3.5 Future revegetation of bare regions

Whether bare regions are suitable for re-vegetation in terms of their ability to sustain future water resources is also a matter of global concern. The difference between annual water supply and evapotranspiration for bare regions has increased only slightly over the past 40 years, and is likely to continue increasing by 32 ± 9 mm during 2030–2100 according to the basic Shared Socio-economic Pathways Scenarios of CMIP6 (Fig. 6a). The increased water availability in the permafrost regions of northern Russia, northern

590 Canada, Greenland, south of the Sahara desert, and the Qinghai-Tibet Plateau offers
591 significant potential for revegetation efforts in these areas. This change could enhance
592 water resources, supporting ecological restoration and habitat development in regions
593 previously limited by harsh conditions. Given that population density is currently very
594 sparse in bare regions (4.5 persons per km^2 on average), it is unlikely that there will be
595 many conflicts in water demand between vegetation and human usage if revegetation
596 is implemented. Soil water storage is expected to be abundant in permafrost areas,
597 which is also helpful in supporting vegetation growth. Moreover, the global land surface
598 temperature is predicted to increase by 3.1 ± 0.7 ℃ by the end of the 21st century based
599 on projections from the 20 CMIP6 models under SSP245, and is amenable to vegetation
600 growth [50]. Therefore, bare regions in permafrost areas are likely to have a large future
601 potential for revegetation.
602
603 In order to estimate the maximum possible fraction of future vegetation cover in
604 different regions of the world, we established a linear regression relationship ($P < 0.01$,
605 Fig. S18 online) between historical change in vegetation cover fraction and the
606 corresponding change in water consumption by vegetation. By assuming this
607 relationship is also valid for the future period, we estimate the potential for future
608 revegetation based on the future change in water consumption. Importantly, we
609 incorporated critical constraints from both soil properties and climatic treeline
610 conditions. Our analysis reveals that future afforestation-suitable bare lands exhibit soil
611 characteristics (including soil organic carbon, pH, nitrogen content, and cation
612 exchange capacity) and climatic treeline conditions comparable to those of existing
613 successfully revegetated regions. This multi-factor validation confirms the robustness
614 of our identified afforestation areas, as they simultaneously satisfy all essential

thresholds for water availability, soil suitability, and thermal growing conditions. The methodological approach ensures that our estimates of afforestation potential reflect not only hydrological feasibility but also account for key ecological constraints that determine long-term vegetation establishment and survival. This comprehensive framework provides a more realistic assessment of global revegetation opportunities under changing environmental conditions.

The results indicate that the potential for future re-vegetation could be up to 1.6% of total bare land areas (40.6×10^4 km^2, Fig. 6b), primarily located in the bare lands of Canada, Central Asia, and the fringes of deserts. These regions thus have potential for vegetation restoration during 2030–2100, playing a significant role in future carbon sequestration efforts.

4 Conclusions

This work identifies revegetated areas of the globe that could evolve from bare regions to vegetated landscapes. Most of these regions show an increasing trend in water consumption for vegetation growth and atmospheric evaporative demand, primarily driven by heightened transpiration. Our analysis of global revegetated regions reveals a complex picture of water resource sustainability. On an annual scale, most revegetated regions exhibit a sustainable balance in regions where water supply from rainfall and meltwater has historically exceeded water consumption by vegetation and humans. Projections for 2030 to 2100 suggest that this trend is likely to continue, supporting both vegetation growth and human water use. However, a closer examination at the monthly scale uncovers significant challenges. Many revegetated regions face critical water stress during peak periods when vegetation demands coincide with high human

consumption, particularly in the irrigation and hydropower sectors. Approximately 44% of these areas experience monthly natural water surpluses that are insufficient to meet human needs, resulting in reliance on local water sources and leading to unsustainable conditions. These insights underscore the importance of considering both annual and monthly scales in water resource management. They highlight the importance of adopting strategies that address seasonal variability in water demand and availability to effectively support both ecological health and human water needs. Finally, we also examined the potential impacts of future vegetation restoration on currently bare land areas. We find water resources in Canada, Central Asia, and the fringes of deserts could support up to 1.6% additional revegetation given the substantial changes in rainfall patterns and the rapid thawing of permafrost land.

This study provides critical insights for policymakers and land managers to optimize revegetation strategies while ensuring water security in a changing climate. However, several limitations and uncertainties remain: although bias correction methods were employed to reduce uncertainties in climate projections, CMIP6 models did not incorporate human water use when simulating regional climate change, which may affect local climate projections. The human water use predictions were based on static sectoral water use and did not account for the potential impacts of global dietary changes on agricultural water demand. Additionally, due to the lack of high-precision global-scale data, the monthly water stress analysis did not consider the mitigating effects of reservoir operations on water scarcity risks (as the study areas had relatively few reservoirs). The potential regulatory effects of future water-saving technologies or water rights reforms on water supply and demand assessments were also not quantified.

Future research should prioritize the development of an integrated "climate-water-society" modeling framework that dynamically couples human interventions (e.g., reservoir operations) with CMIP6 downscaling to analyze the feedback effects of water resource use on local climate. Simultaneously, dietary transition scenarios should be incorporated to refine agricultural water demand projections in revegetation-agriculture nexus regions. Furthermore, policy-sensitive modules should be embedded to evaluate the synergistic effects of water-saving technologies and institutional reforms, quantifying their potential contributions to alleviating monthly water stress, and ultimately providing spatially explicit decision support for sustainable revegetation in evolving socioeconomic contexts.

Data availability

The CMIP6 simulations data is available from https://aims2.llnl.gov/search/cmip6/. Monthly data on transpiration and interception losses, bare soil evaporation, snow sublimation, and open water evaporation are derived from the Global Land Evaporation Amsterdam Model datasets (GLEAM) at a spatial resolution of 0.25°× 0.25°(https://www.gleam.eu/). The observed Leaf Area Index data is available from https://www.ncei.noaa.gov/access/metadata/landing-page/bin/iso?id=gov.noaa.ncdc:C01559. Monthly precipitation data is obtained from the Global Precipitation Climatology Centre (GPCC) (https://climatedataguide.ucar.edu/climate-data/gpcc-global-precipitation-climatology-centre). Monthly meltwater data is collected from ERA5-land (https://cds.climate.copernicus.eu/datasets). Data on the monthly human water consumption was obtained from https://dataverse.harvard.edu/dataset.xhtml?persistentId=doi:10.7910/DVN/VIQEAB.

Monthly data of temperature and actual vapor pressure are collected from https://data.ceda.ac.uk/badc/cru/data/cru_ts/cru_ts_4.01/. The data for evapotranspiration, precipitation, temperature, and snowmelt water were collected from the ERA5-Land dataset (https://cds.climate.copernicus.eu/datasets/reanalysis-era5-land-monthly-means?tab=overview). Soil parameter data (including soil carbon stock, pH values, cation exchange capacity, and nitrogen content) were obtained from SoilGrids (https://soilgrids.org/).

Acknowledgements

Valuable comments from Dr. Shan Zheng in Wuhan University, and Dr. Han Dolman and Dr. Naudts Kim in Vrije Universiteit Amsterdam are acknowledged. The authors are also grateful to Mr. Ruilin Xu in Wuhan University for enhancing Fig. 1 in the main text. This work is supported by the National Natural Science Foundation of China (No. U24A20572, No. 42301018) and the National Key Research and Development Program of China (No. 2024YFF0809301, No. 2024YFE0214000).

Author Contributions

Yuanfang Chai, Yao Yue, and Chiyuan Miao conceived and designed the research, developed the methodology, and wrote the original draft. Yichu Wang and Yuanfang Chai conducted the investigation. Alistair GL Borthwick, Louise Slater, Yichu Wang, Dunxian She, and Dongpu Feng reviewed and edited the manuscript. Yao Yue and Chiyuan Miao supervised the project.

Conflict of interest

The authors declare no competing interests.

Additional information

Correspondence and requests for materials should be addressed to Yao Yue and Chiyuan Miao.

References

[1] Deng Q, McMahon D E, Xiang Y, et al. A global meta-analysis of soil phosphorus dynamics after afforestation. New Phytol 2017; 213: 181–92.
[2] Zheng H, Miao C, Huntingford C, et al. The impacts of erosion on the carbon cycle. Rev Geophys 2025; 63: e2023RG000829.
[3] Gao Y, Li X, Liu L, et al. Seasonal variation of carbon exchange from a revegetation area in a Chinese desert. Agr Forest Meteorol 2012; 156: 134–42.
[4] Wang X P, Pan Y X, Zhang Y F, et al. Temporal stability analysis of surface and subsurface soil moisture for a transect in artificial revegetation desert area, China. J Hydrol 2013; 507: 100–9.
[5] Song X P, Hansen M C, Stehman S V, et al. Global land change from 1982 to 2016. Nature 2018; 560: 639–43.
[6] Bastin J F, Finegold Y, Garcia C, et al. The global tree restoration potential. Science 2019; 365: 76–9.
[7] Chai Y, Miao C, Slater L, et al. Underestimating global land greening: Future vegetation changes and their impacts on terrestrial water loss. One Earth 2025; 8: 101176.
[8] Farley K A, Jobbágy E G, Jackson R B. Effects of afforestation on water yield: a global synthesis with implications for policy. Global Change Biol 2005; 11: 1565–76.
[9] Lu C, Zhao T, Shi X, et al. Ecological restoration by afforestation may increase groundwater depth and create potentially large ecological and water opportunity costs in arid and semiarid China. J Clean Prod 2018; 176: 1213–22.
[10] Feng X, Fu B, Piao S, et al. Revegetation in China's Loess Plateau is approaching sustainable water resource limits. Nat Clim Change 2016; 6: 1019–22.
[11] Brown A E, Zhang L, McMahon T A, et al. A review of paired catchment studies for determining changes in water yield resulting from alterations in vegetation. J Hydrol 2005; 310: 28–61.
[12] Chen Y, Wang K, Lin Y, et al. Balancing green and grain trade. Nat Geosci 2015; 8: 739–41.
[13] Roundy B A, Farmer M, Olson J, et al. Runoff and sediment response to tree control and seeding on a high soil erosion potential site in Utah: evidence for reversal of an abiotic threshold. Ecohydrology 2017; 10: e1775.
[14] Zhang S, Yang D, Yang Y, et al. Excessive afforestation and soil drying on China's Loess Plateau. J Geophys Res-Biogeo 2018; 123: 923–35.
[15] Zastrow, M. China's tree-planting drive could falter in a warming world. Nature 2019; 573: 474–475.
[16] Makarieva A M, Gorshkov V G, Li B L. Conservation of water cycle on land via restoration of natural closed-canopy forests: implications for regional landscape planning. Ecol Res 2006; 21: 897–906.

[17] Zhang K, Kimball J, Nemani R, et al. Vegetation greening and climate change promote multidecadal rises of global land evapotranspiration. Sci Rep-Uk 2015; 5: 15956.
[18] Li Y, Piao S, Li L Z, et al. Divergent hydrological response to large-scale afforestation and vegetation greening in China. Sci Adv 2018; 4: eaar4182.
[19] Podrazsky V, Holubík O, Vopravil J, et al. Effects of afforestation on soil structure formation in two climatic regions of the Czech Republic. J For Sci-Prague 2015; 61: 225–34.
[20] Yosef G, Walko R, Avisar R, et al. Large-scale semi-arid afforestation can enhance precipitation and carbon sequestration potential. Sci Rep-Uk 2018; 8: 996.
[21] Piao S, Friedlingstein P, Ciais P, et al. Effect of climate and CO_2 changes on the greening of the Northern Hemisphere over the past two decades. Geophys Res Lett 2006; 33: L23402.
[22] Cao S, Zhang J, Chen L, et al. Ecosystem water imbalances created during ecological restoration by afforestation in China, and lessons for other developing countries. J Environ Manage 2016; 183: 843–49.
[23] Panagos P, Borrelli P, Meusburger K, et al. Estimating the soil erosion cover-management factor at the European scale. Land Use Policy 2015; 48: 38–50.
[24] Martens B, Miralles D G, Lievens H, et al. GLEAM v3: Satellite-based land evaporation and root-zone soil moisture. Geosci Model Dev 2017; 10: 1903–25.
[25] Zhang G, Yao T, Xie H, et al. Response of Tibetan Plateau lakes to climate change: Trends, patterns, and mechanisms. Earth-Sci Rev 2020; 208: 103269.
[26] Khan Z, Thompson I, Vernon C R, et al. Global monthly sectoral water use for 2010–2100 at 0.5° resolution across alternative futures. Sci Data 2023; 10: 201.
[27] Huang Z, Hejazi M, Li X, et al. Reconstruction of global gridded monthly sectoral water withdrawals for 1971–2010 and analysis of their spatiotemporal patterns. Hydrol Earth Syst Sc 2018; 22: 2117–33.
[28] Mekonnen M M, Hoekstra A Y. Total monthly blue water footprints of production at a 30 × 30 arc minute grid resolution (1996–2005). https://waterfootprint.org/en/resources/waterstat/monthly-gridded-blue-water-footprint-statistics/ (2011).
[29] Chai Y, Yue Y, Slater L J, et al. Constrained CMIP6 projections indicate less warming and a slower increase in water availability across Asia. Nat Commun 2022; 13: 4124.
[30] Zhou L, Jiang Z H. Future changes in precipitation over Hunan Province based on CMIP5 simulations using the statistical downscaling method of transform cumulative distribution function. Acta Meteorol Sin 2017; 75: 223–35.
[31] Kojwang H O, Larwanou M. Forestry-related input into relevant policies at the regional and global levels: an African perspective on climate change. Int Forest Rev 2015; 17: 92–102.
[32] Basu J P. Agroforestry, climate change mitigation and livelihood security in India. Nz J Forestry Sci 2014; 44: S11.
[33] Yao Z, Zhang L, Tang S, et al. The basic characteristics and spatial patterns of global cultivated land change since the 1980s. J Geogr Sci 2017; 27: 771–85.
[34] Stendel M, Christensen J H. Impact of global warming on permafrost conditions in a coupled GCM. Geophys Res Lett 2002; 29: 10-1–10-4.
[35] Wang X, Yi S, Wu Q, et al. The role of permafrost and soil water in distribution of alpine grassland and its NDVI dynamics on the Qinghai-Tibetan Plateau. Global Planet Change 2016; 147: 40–53.
[36] Liu Y, Xiao J, Ju W, et al. Recent trends in vegetation greenness in China

809 significantly altered annual evapotranspiration and water yield. Environ Res Lett
810 2016; 11: 094010.
811 [37] Azorin-Molina C, Vicente-Serrano S M, Sanchez-Lorenzo A, et al. Atmospheric
812 evaporative demand observations, estimates and driving factors in Spain (1961–
813 2011). J Hydrol 2015; 523: 262–77.
814 [38] Berg A, Findell K, Lintner B, et al. Land–atmosphere feedbacks amplify aridity
815 increase over land under global warming. Nat Clim Change 2016; 6: 869–74.
816 [39] Jung M, Reichstein M, Ciais P, et al. Recent decline in the global land
817 evapotranspiration trend due to limited moisture supply. Nature 2010; 467: 951–4.
818 [40] Schuur E A, McGuire A D, Schädel C, et al. Climate change and the permafrost
819 carbon feedback. Nature 2015; 520: 171–9.
820 [41] Chasmer L, Hopkinson C. Threshold loss of discontinuous permafrost and
821 landscape evolution. Global Change Biol 2017; 23: 2672–86.
822 [42] Warren R K, Pappas C, Helbig M, et al. Minor contribution of overstorey
823 transpiration to landscape evapotranspiration in boreal permafrost
824 peatlands. Ecohydrology 2018; 11: e1975.
825 [43] Zhu L, Gong H, Dai Z, et al. An integrated assessment of the impact of
826 precipitation and groundwater on vegetation growth in arid and semiarid areas. Environ
827 Earth Sci 2015; 74: 5009–21.
828 [44] Zhang W, Hu G, Dang Y, et al. Afforestation and the impacts on soil and water
829 conservation at decadal and regional scales in Northwest China. J Arid Environ 2016;
830 130, 98–104.
831 [45] Peng S, Piao S, Ciais P, et al. Change in winter snow depth and its impacts on
832 vegetation in China. Global Change Biol 2010; 16: 3004–13.
833 [46] Previdi M. Radiative feedbacks on global precipitation. Environ Res Lett 2010; 5:
834 025211.
835 [47] Lee X, Goulden M L, Hollinger D Y, et al. Observed increase in local cooling
836 effect of deforestation at higher latitudes. Nature 2011; 479: 384–387.
837 [48] Wang Z, Wu R, Chen Z, et al. Reasons for East Siberia winter snow water
838 equivalent increase in the recent decades. Remote Sens-Basel 2023; 15: 134.
839 [49] Khan Z, Thompson I, Vernon C R, et al. Global monthly sectoral water use for
840 2010–2100 at 0.5° resolution across alternative futures. Sci Data 2023; 10: 201 .
841 [50] Yi Y, Kimball J S, Rawlins M A, et al. The role of snow cover affecting boreal-
842 arctic soil freeze-thaw and carbon dynamics. Biogeosciences 2015; 12: 5811–29.
843
844 **Figure captions:**

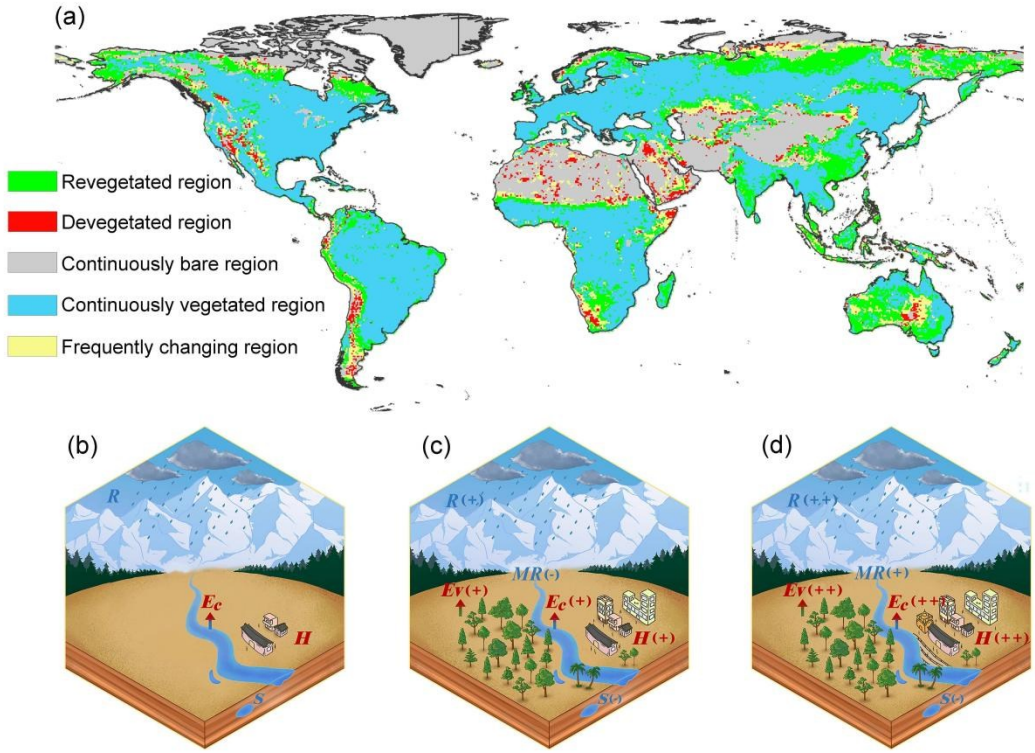

Figure 1. Schematic of the historical changes in water supply and consumption before and after revegetation during 1982–2016; (a) Classification of land cover is as follows: Revegetated regions are lands that have been altered from bare to vegetated; Devegetated regions, from vegetated to bare; Continuously Bare regions, with a cover fraction < 10% throughout 1982–2016; Continuously Vegetated regions, with a cover fraction > 10% throughout 1982–2016; Frequently Changing regions, with continuous changes in land cover between bare and vegetated. (b) shows the water balance before revegetation activities during 1982–2016; (c) shows the changes in water consumption and supply after revegetation during 1982–2016; (d) shows the changes in water consumption and supply in the future (2030–2100); *R* (Rainfall) and *MR* (melting water from snow and glaciers) are the main sources of water supply; *Ec* (evaporation meeting atmospheric evaporative demand), *Ev* (transpiration and interception losses), and *H* (human water use) are the primary pathways of water consumption; *S* indicates soil water content. Increasing/decreasing trends are represented by plus/minus signs (+/-). If the increasing/decreasing trend is projected to continue during the future period, we use ++/-- in (c).

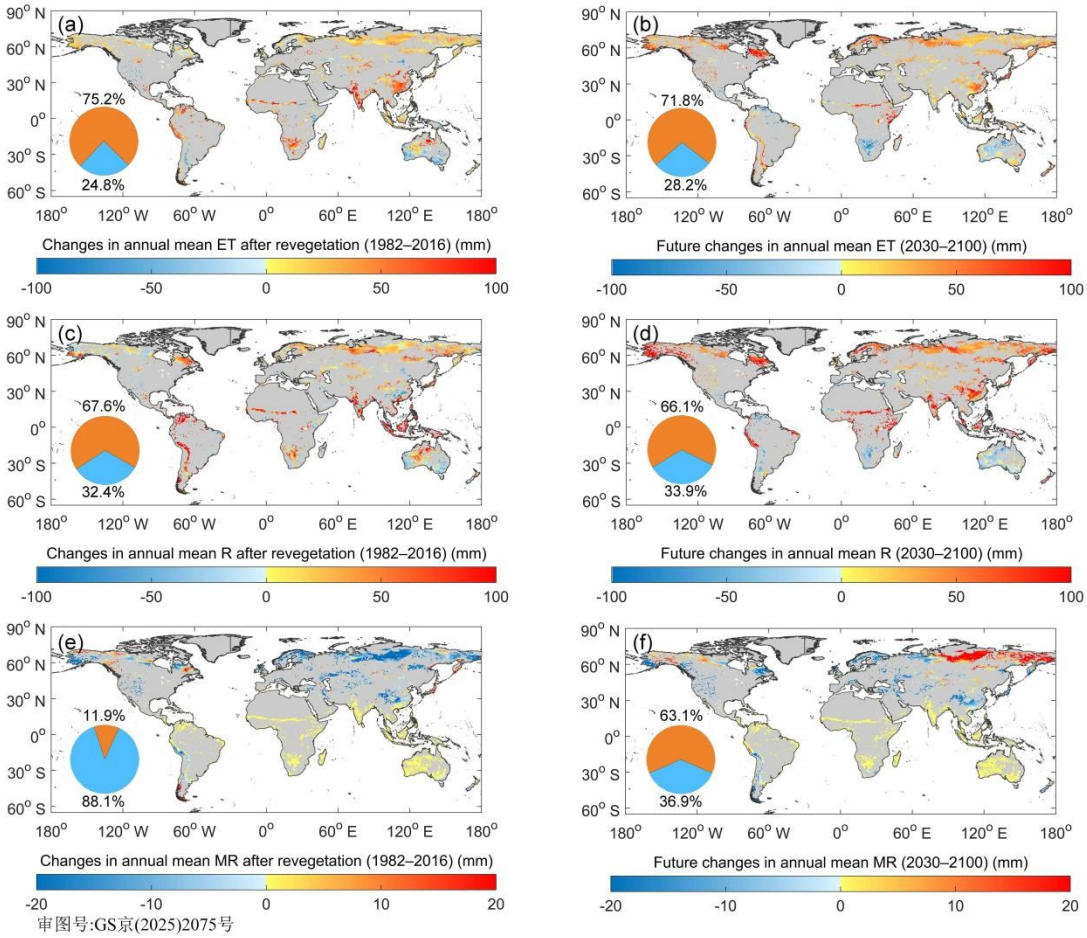

Figure 2. Changes in annual mean water supply and consumption from 1982 to 2016 and projections from 2030 to 2100. (a), (c) and (e) show the changes in annual mean evapotranspiration (ET), rainfall (R), and meltwater from snow and glaciers (MR) by comparing conditions before and after revegetation during 1982 to 2016. (b), (d) and (f) present changes in these three variables by comparing projections for 2030 to 2100 with the post-revegetation conditions established in 1982 to 2016. Inset pie charts show the proportions of decrease (blue) and increase (red).

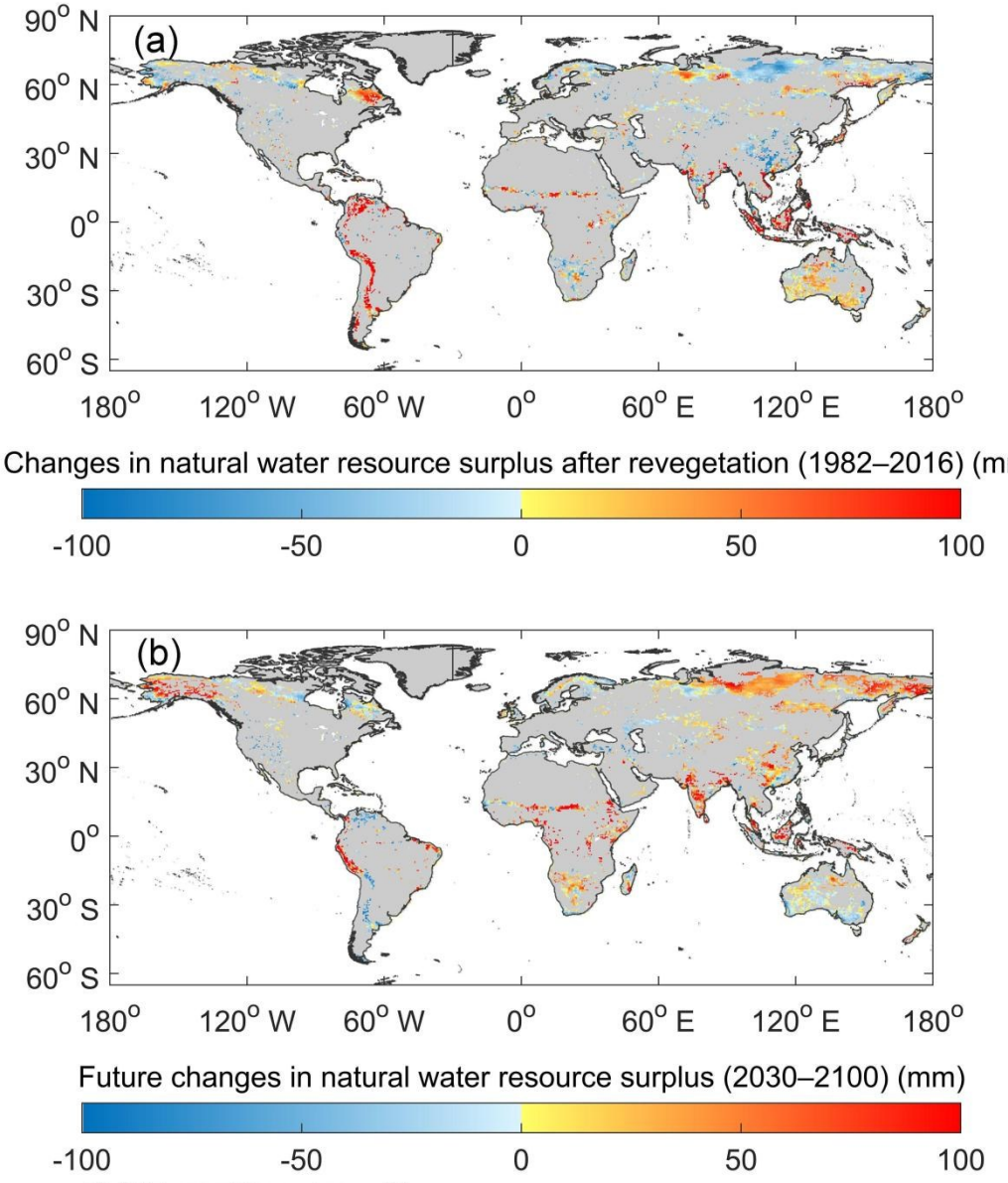

Figure 3. Changes in the difference between water supply and natural water consumption by vegetation (natural water surplus) from 1982 to 2016 and projections from 2030 to 2100. (a) shows the changes in annual mean natural water surplus by comparing conditions before and after revegetation during 1982 to 2016. (b) presents changes in annual mean natural water surplus by comparing projections for 2030 to 2100 with the post-revegetation conditions established in 1982 to 2016.

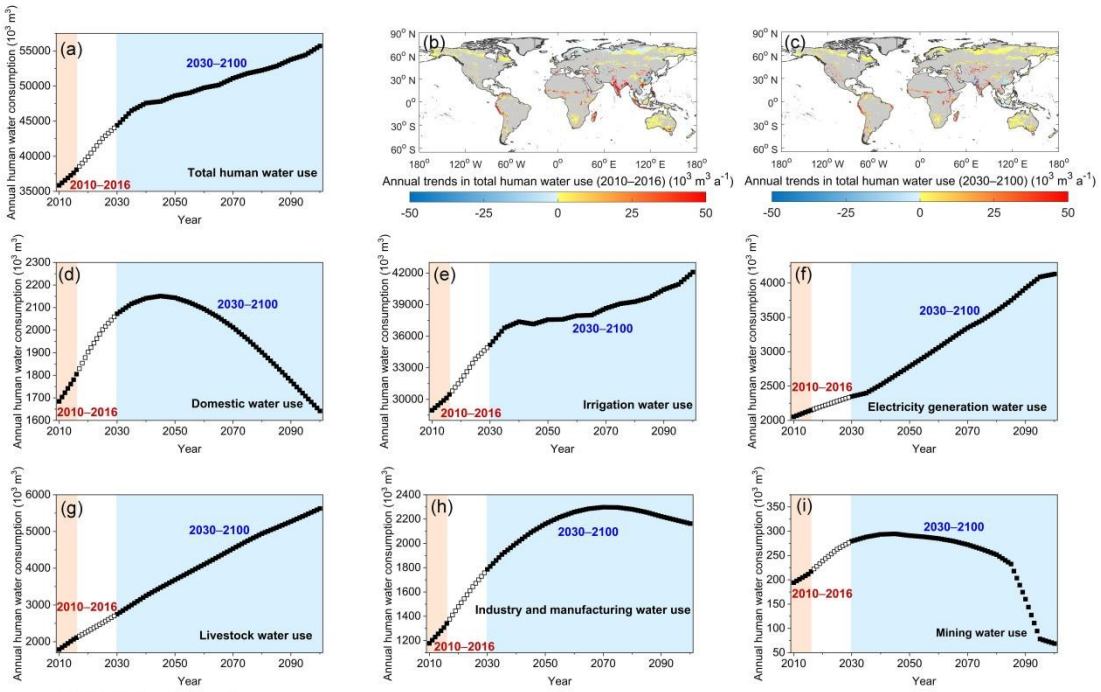

Figure 4. Changes in annual human water consumption from 2010 to 2100. (a) presents the time series of total annual human water consumption. (b) and (c) show annual variations in total human water consumption during 2010–2016 and 2030–2100, respectively. (d) to (i) represent the time series of domestic water use (d), irrigation water use (e), electricity generation water use (f), livestock water use (g), industrial and manufacturing water use (h), and mining water use (i), respectively. 2010–2016 corresponds to the observed period, whereas 2030–2100 reflects the CMIP6 projections under SSP245.

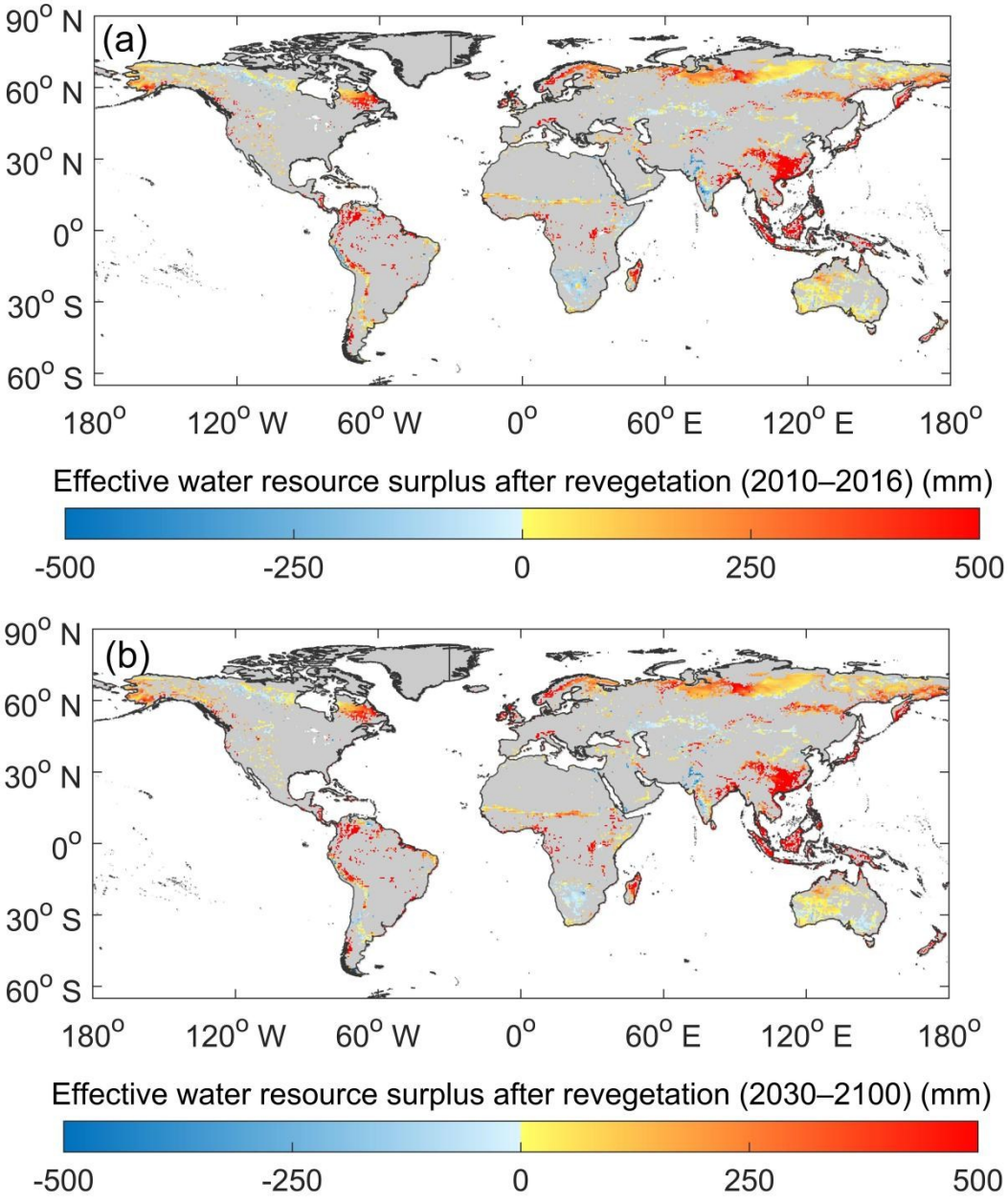

Figure 5. Difference between water supply and water consumption by vegetation and humans (effective water surplus) during 2010–2016 (historical observations) and 2030–2100 (projections). (a) shows annual mean effective water surplus obtained by subtracting water consumption by vegetation and humans from the total water supply comprising rainfall and meltwater from snow and glaciers after revegetation in 2010–2016. Since data on human water consumption is unavailable prior to 2010, this analysis focuses solely on the period from 2010 to 2016. (b) presents the annual mean effective water resource surplus projected for 2030–2100.

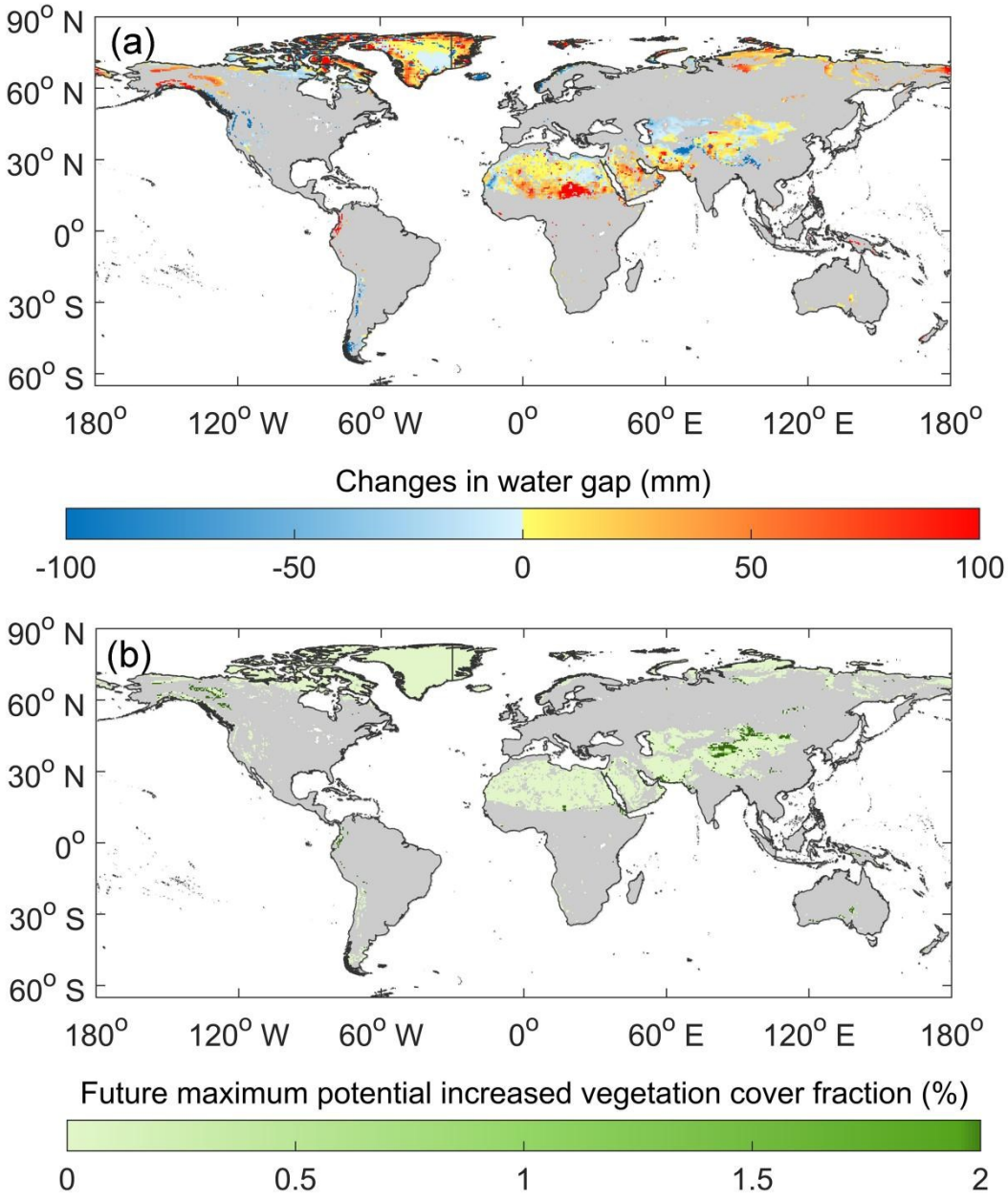

Figure 6. Future potential for increased vegetation cover fraction in bare land regions based on increased water gap between water supply and consumption. (a) shows the changes in the water gap (ΔW, mm) between water supply and water consumption. It compares the average future conditions (from 2030 to 2100) with historical conditions (from 1982 to 2016). (b) shows the maximum potential increase in vegetation cover fraction (ΔCF, %) in sustainable areas of bare regions projected for the period from 2030 to 2100.